JCTC Journal of Chemical Theory and Computation

Article

pubs.acs.org/JCTC

Specific Conformational States of Ras GTPase upon Effector Binding

Julie Baussand* and Jens Kleinjung

Division of Mathematical Biology, MRC National Institute for Medical Research, The Ridgeway, Mill Hill, London NW7 1AA, United Kingdom

Supporting Information

ABSTRACT: To uncover the structural and dynamical determinants involved in the highly specific binding of Ras GTPase to its effectors, the conformational states of Ras in uncomplexed form and complexed to the downstream effectors Byr2, PI3Kγ, PLCε, and RalGDS were investigated using molecular dynamics and cross-comparison of the trajectories. The subtle changes in the dynamics and conformations of Ras upon effector binding require an analysis that targets local changes independent of global motions. Using a structural alphabet, a computational procedure is proposed to quantify local conformational changes. Positions detected by this approach were characterized as either specific for a particular effector, specific for an effector domain type, or as effector unspecific. A set of nine structurally connected residues (Ras residues 5−8, 32−35, 39−42, 55−59, 73−78, and 161−165), which link the effector binding site to the distant C-terminus, changed dynamics upon effector binding, indicating a potential effector-unspecific signaling route within the Ras structure. Additional conformational changes were detected along the N-terminus of the central β-sheet. Besides the Ras residues at the effector interface (e.g., D33, E37, D38, and Y40), which adopt effector-specific local conformations, the binding signal propagates from the interface to distant hot-spot residues, in particular to Y5 and D57. The results of this study reveal possible conformational mechanisms for the stabilization of the active state of Ras upon downstream effector binding and for the structural determinants responsible for effector specificity.

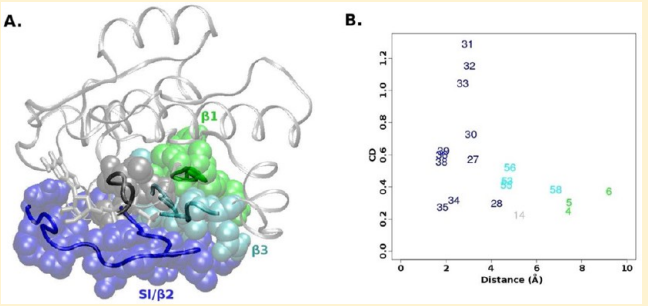

INTRODUCTION

Ras proteins are guanosine nucleotide-dependent molecular switches that act at the inner surface of cell membranes to control signaling pathways involved in cell proliferation, growth, and development. Activating mutations of Ras genes are common in tumor development and cancer.[1] Ras GTPase binds to several downstream effectors, and its key role in the activation of multiple important biological pathways in the cell requires a tight regulation of its activity. The biological activity of Ras is controlled by a GDP/GTP cycle that modulates the conformation of Ras and thereby its affinity for downstream effectors. Ras proteins cycle between a GDP-bound and a GTP-bound form. The GDP-bound Ras is an inactive conformation incapable of effector binding. The GTP-bound form exists in a conformational equilibrium between state2 and state1. State2 is the active form that is able to execute downstream signaling through direct interaction with its effectors such as phosphoinositide 3-kinases (PI3Kγ), Byr2, Ral guanine nucleotide dissociation stimulator (RalGDS), and phospholipase Cε (PLCε),[2] while state1 displays a 20-fold lower affinity for effectors than state2.[3] Structurally, Ras GDP-bound and GTP-bound state1 share similar differences to the active Ras GTP-bound state2.[4] Ras GTP-bound state2 corresponds to a closed conformation in which the two functional loops switch I (SI) and switch II (SII) interact with the γ-phosphate (γ-P) of GTP. In the GDP-bound and GTP-bound state1 forms, Ras adopts an open conformation marked by a detachment of SI from the guanosine nucleotide, leading to an increased flexibility of SI and SII.[4] The conformational changes of the switch regions in the GDP/GTP transition are characterized by correlated motions between elements of the N-terminal nucleotide-binding subdomain and C-terminal subdomain.[5] These changes play a role in the nucleotide-dependent orientation of the catalytic domain of Ras relative to the membrane, which has been shown to critically affect effector binding.[6] In the active closed conformation, the catalytic domain is stabilized in an orientation that facilitates effector binding to SI.[7,8]

Active Ras binds specifically to a range of downstream effectors. Although all known downstream effectors of Ras share a common ubiquitin-like binding domain (classified as Ras Binding (RB) or Ras Association (RA) domains[9]), not all ubiquitin-like domains interact with Ras GTPases. Contrarily, Ras discriminates even between various isoforms of its effectors.[10] A set of positively charged residues at the surface of true RA/RB domains has been shown to be required for Ras binding.[11,12] Mutation analyses have revealed single point mutations within the effector binding region of Ras (residues 32−40) that can selectively affect effector interactions.[10,13]

Received: August 17, 2012
Published: November 6, 2012

   dx.doi.org/10.1021/ct3007265 | J. Chem. Theory Comput. 2013, 9, 738−749

Furthermore, it has been demonstrated that two point mutations suffice to produce switch-of-function mutants between different branches of the Ras superfamily. One of these point mutations is distant from the effector binding surface, which suggests an allosteric control of selective effector binding.[14] Also dynamics trajectories of free Ras and Ras bound to Raf highlighted changes in the mobility of regions far from the binding interface,[15] but it is not clear whether these changes in Ras dynamics are common to all effectors or are effector-specific. Thermodynamic analyses confirmed significant free energy contributions from residues that are distant from the complex interface[16,17] and the specificity of the respective Ras:RalGDS and Ras:Raf interactions.[18,19]

The comparison of structurally resolved Ras:effector complex structures shows a close structural similarity: formation of an antiparallel β-sheet between β2 of the effector binding domain and β2 of Ras, which induces minor conformational changes in both proteins.[20−23] Only a few degrees of rotation angle difference around the β2-sheet axis were observed between the effectors Raf, RalGDS, PI3Kγ, and Byr2. These differences are assumed to be related to the length of the loops connecting the effector's interacting β-sheet.[24] More pronounced differences may arise from the analysis of Ras dynamics since it has been shown to play a major role in the recognition mechanism.[25] Moreover, changes of flexibility in complexes are key events for the activation of downstream effectors in other proteins of the Ras superfamily.[26] Questions regarding the influence of effector binding on the dynamics and conformational ensembles of Ras and the specificity of these influences are still open. It is clear that the dynamics of the SI region are critical for effector binding;[3,27] less is known about the global flexibility of Ras in its effector complexes, although it is very likely to invoke an allosteric mechanism to propagate the complexation signal through the Ras structure. The decrease of atomic fluctuations of hot-spot residues (i.e., residues that make a dominant contribution to the free energy of protein−protein binding) upon binding with Raf and RalGDS[16] show the functional importance of flexibility in the binding process. The pathways from the effector binding site to the hot-spot residues further distant from the interface are yet unknown. Only weak correlations have been found between the location of conformational changes and the location of the hot-spot residues. However, even small conformational changes may be energetically relevant; for example, Ras−D57 undergoes only minor conformational changes upon RalGDS and Raf association, but it is detected as a hot-spot residue in both complexes.[16]

Our current understanding of the rather complex interplay between the Ras structure and its functional activity *via* the complexation with downstream effectors requires more information about the dynamic processes involved. Particularly local conformational changes are of interest, because some global metrics such as RMSD (root-mean-square deviation) are often dominated by roto-translational contributions from loops that are not necessarily correlated with the biological function. Here, we present an analysis of the molecular dynamics of five Ras GTP-loaded systems, one unbound and four bound to the effectors PI3Kγ, Byr2, PLCε, and RalGDS. For each of the five systems, three replicate simulations of 100 ns were performed and analyzed in terms of local and global conformational changes along the trajectories. For global analysis, RMSD, RMSF (root-mean-square fluctuation), conformational clustering, and contact maps were computed. For local analysis, a structural alphabet-based approach is proposed. It quantifies local changes between pairs of conformational ensembles. The comparison is performed between simulations of the same system and between those of different systems, which allows us to evaluate the intersystem changes versus the intrasystem changes. The results of both local and global analysis show a combination of effector-specific and effector-unspecific modifications of the conformations and dynamics of the catalytic domain of Ras. A communication path between the SI region and the membrane interacting C-terminus was detected, which is possibly involved in the stabilization of the active state2 of Ras upon downstream effector binding. Moreover, conformational differences between the different effector complexes of Ras were detected at positions previously shown to be functionally important by mutation experiments. Their analysis provides additional molecular insights into effector-specific binding modes.

METHODS

Structures and Models. Five structures of GTP-loaded Ras (H-Ras isoform) were selected, one unbound (PDB 1qra[28]) and four in complex with the following downstream effectors: PI3Kγ (PDB 1he8[22]), RalGDS (PDB 1lfd[29]), PLCε (PDB 2c5l[30]), and Byr2 (PDB 1k8r[23]), the *S. pombe* functional homologue of Raf. The original PDB structures were modified to obtain suitable and comparable starting structures for simulations, partly to correct for substitutions and missing coordinates in the experimental structures. The entire catalytic domain (residues 1−166) and the effector binding domain (residues 1he8A:217−310, 1lfdA:14−100, 2c5lC:2134−2238, 1k8rB:71−165) were selected from the PDB structures. Using MODELLER,[31] the mutations 1qrA:G12V, 1he8A:G12V, 1he8B:V223K, 1lfdA:E32K, and 2c5lA:G12V of the PDB structures were reversed to wild-type Ras. The missing coordinates of loops 1k8rB:122−142 in Byr2 and 2c5lC:2189−2211 in PLCε were modeled using residues 1i35A:52−72 in uncomplexed Byr2 and 2byfA:60−81 in uncomplexed PLCε as a template. Models with the lowest DOPE (Discrete Optimised Protein Energy) score were selected.[32] GNP (phosphoaminophosphonic acid guanylate ester), a nonhydrolyzable GTP analogue, was modified to GTP in the respective complexes.

In the following, Ras unbound is referred to as Ras^{U} and Ras bound to any of the four effectors studied here is collectively referred to as Ras^{B}. Ras in complex with individual effectors is denoted Ras^{Byr2}, $Ras^{PI3K\gamma}$, $Ras^{PLC\varepsilon}$, and Ras^{RalGDS}, while the complexes themselves are denoted Ras:Byr2, Ras:PI3Kγ, Ras:PLCε, and Ras:RalGDS.

Molecular Dynamics. Molecular Dynamics (MD) simulations were performed using the GROMACS package[33] with the G43a1 force field. Proteins were solvated in a cubic box with SPC water molecules;[34] the box size was set to ensure a distance of at least 15 Å between the protein and the box boundaries. Systems were neutralized using counterions. All systems were subjected to 1000 steps of steepest-descent energy minimization. Gradually decreasing positional restraints were imposed on the heavy atoms during constant volume heating from 200 to 300 K and equilibration for 100 ps. An additional unconstrained 200 ps of equilibration was performed at 300 K and 1 atm. Simulations were run for 100 ns at a constant temperature (300 K) and pressure (1 bar). The temperature was controlled by weak coupling to a temperature bath[35] with a coupling constant τ_T = 0.1 ps. Bond lengths were

dx.doi.org/10.1021/ct3007265 | J. Chem. Theory Comput. 2013, 9, 738−749

constrained by the SHAKE algorithm.[36] The nonbonded pair list was updated every time step for pairs within 0.8 nm and every fifth time step for the range 0.8−1.4 nm. Twin-range cutoff radii of 0.8/1.4 nm were used to compute nonbonded interactions. Long-range electrostatic interactions were approximated by a reaction-field force, using a dielectric constant of 54. Simulations in explicit water were kept at 0.061020 kJ mol^{-1} nm^{-3} (1 atm) with a coupling time of τ_P = 0.5 ps and an isothermal compressibility of 5.575×10^{-4} (kJ mol^{-1} $nm^{-3})^{-1}$. Electrostatic interactions were evaluated using the Particle Mesh Ewald sum with a cutoff of 14 Å. The integration time step width was 2 fs. Conformational snapshots were saved at 1 ps intervals. For each of the five systems, three independent 100 ns simulations were run using identical parameters except for the random initial velocities.

Contact Maps. For each pair of residues, the distance between the constituting atoms was computed every 100 ps (i.e., 1000 structures *per* trajectory). A pair of residues was defined to be in contact if at least two of their constituting atoms were closer than 4 Å. For intramolecular contact maps, the number of residue contacts was reported for each pair of Ras residues. To ensure a consistent comparison between the different systems, only the *persistent* contacts were considered, i.e., those occurring in at least 50% of the 1000 conformations in each of the three simulation replicates, as proposed by Gorfe et al.,[37] leading to one contact map per system. For intermolecular contact maps, the largest number of contacts formed by each Ras residue with an effector residue was reported. Intermolecular contact maps were computed to identify potential differences between interacting residues at the Ras interface in the effector complexes.

Structural Alphabet Encoding. M32K25 is a structural alphabet comprising 25 prototypical fragments of four C^{α} atoms labeled by letters [A−Y].[38] The structural alphabet is a coarse-grained representation of the protein backbone that disregards side chain conformations. The structural alphabet M32K25 was derived from a comprehensive map of fragments occurring in high-resolution protein structures, where the points of highest density were extracted as representative conformations (alphabet letters). The rationale behind this selection is that low energy conformations occur most frequently (reverse Boltzmann principle). The size of the alphabet was derived from an extremum in a plot of the Akaike Information Criterion over the alphabet size, i.e., by balancing the number of free parameters against the fit quality. The fit procedure attributes to each four-residue fragment of the Ras structure the most similar fragment (in terms of RMSD) of the structural alphabet. Changes of side chain conformations are detected only if they affect the backbone conformation. M32K25 is used here to encode each MD trajectory as a time-ordered set of structural letter sequences. Encoding is achieved by assigning the most similar prototype fragment of the structural alphabet to each four-residue segment (allowing for overlaps) of the given structure. A character at position i in a structural sequence represents the C^{α} trace conformation at residues i to $i + 3$ of the corresponding structure. Each structural sequence reflects the local conformation of the protein at the given point in time. A trajectory is encoded as a time-ordered set of T sequences of $N - 3$ letters, where T is the number of structures in the trajectory and N is the number of residues in the protein. All 15 trajectories from 5 to 100 ns were encoded into 15 sets of 95 000 structural sequences of 163 letters length.

Structural Sequence Analysis. Using the structural alphabet encoding, a procedure is proposed to quantify local changes between pairs of simulations and to compare these changes within a system (replicates of a given system) and between the systems (replicates of different systems).

Sequence Entropy. The structural letter composition at a given position reflects the ensemble of local conformations adopted by the fragment during the simulation. We used a sequence entropy measure to evaluate the difference in structural letter distribution at a given position between pairs of structural sequence sets. Specifically, we used Sequence Harmony (SH),[39] a metric that yields scores in the value range [0−1]: 0 for maximally dissimilar structural letter distribution and 1 for identical distribution. Let X and Y be the structural sequence sets encoding two trajectories. The SH value of fragment i by comparison of X and Y is computed as

$$\mathrm{SH}_i^{X,Y} = \frac{1}{2}(S_i^{X,Y} - (S_i^X + S_i^Y)) \tag{1}$$

where

$$S_i^{X,Y} = \sum (p_{i,s}^X + p_{i,s}^Y) \log_2(p_{i,s}^X + p_{i,s}^Y) \tag{2}$$

$$S_i^X = \sum p_{i,s}^X \log_2 p_{i,s}^X \tag{3}$$

with $p_{i,s}^X$ being the observed probability of structural letter s at position i in the structural sequence set X.

Hierarchical Clustering of Trajectories. On the basis of the SH values of the comparison between all pairs of considered trajectories, a distance matrix was generated for each Ras fragment. The distance between two trajectories X,Y at a position i was defined as $1 - \mathrm{SH}_i^{X,Y}$. The distance values range between 0 ($\mathrm{SH}_i^{X,Y} = 1$) and 1 ($\mathrm{SH}_i^{X,Y} = 0$). The UPGMA algorithm[40] was applied to each position-specific distance matrix to compute hierarchical clusters based on the similarity between the trajectories at fragment i. Clusters were constructed as binary trees with trajectories as leaves. The closest pair of subclusters (i.e., one trajectory or a subcluster of trajectories) was merged sequentially; the connecting nodes were located in the tree at a height corresponding to half the distance between the two subclusters.

Conformational Cluster Analysis. Each simulated system A was represented in the tree by the smallest subtree whose leaves include the three simulation replicates of system A (referred to as the A-subtree). The systems were compared through their corresponding subtree using two distance-based parameters: the conformational sampling difference ΔCS and the conformational distance CD.

The conformational sampling difference ΔCS between A and B is the difference between the height of the root nodes of their corresponding subtrees, $\Delta\mathrm{CS} = |h(A) - h(B)|$, where $h(A)$ is the height of the root node of the A-subtree. A low root node (high SH values between the replicates) indicates that the fragment explored a similar conformational ensemble in each replicate (converged; Figure S1A), as opposed to a high node, which indicates large differences between the replicates due to a wider conformational sampling (unconverged; Figure S1C). Therefore, ΔCS is indicative of a different sampling width between two systems. The relative sampling width is denoted $\Delta\mathrm{CS}^+$ in the following if $h(A) > h(B)$ and $\Delta\mathrm{CS}^-$ if $h(A) < h(B)$. ΔCS values range from 0 to 1.

The conformational distance CD between A and B is the sum of the branch lengths separating the root node of their

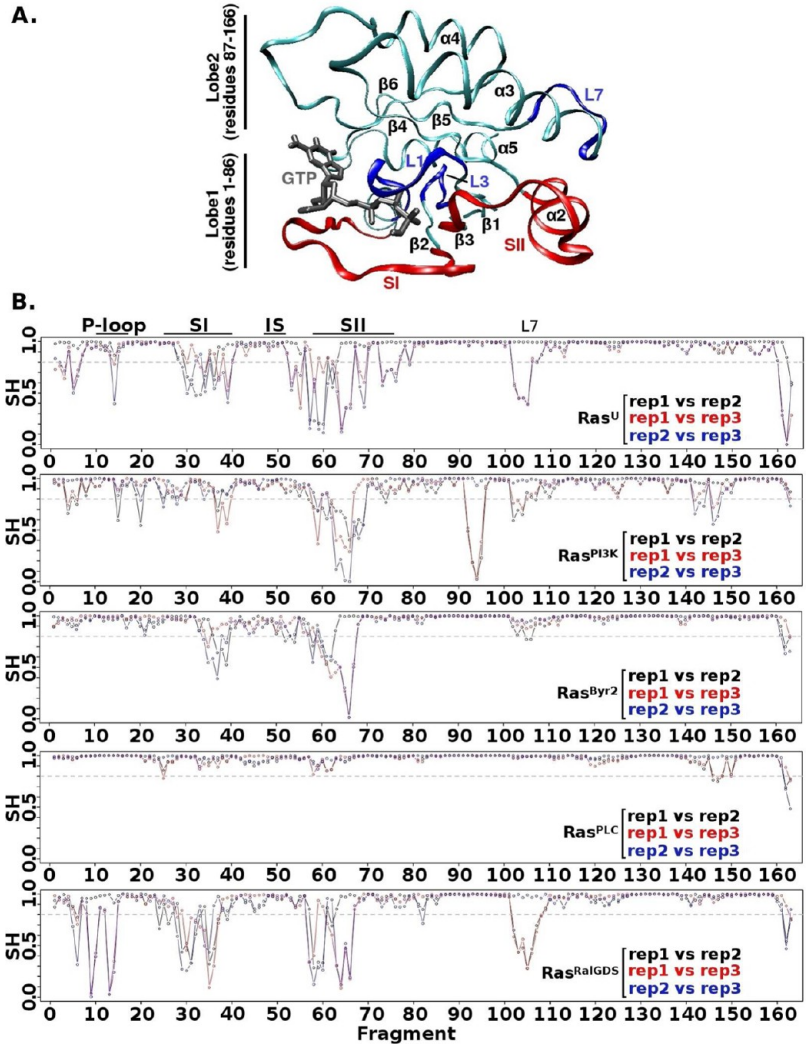

Figure 1. (A) Ras structure. The six β-strands and the five α-helices are labeled. The two switch regions are colored in red: SI encompasses L2 and the N-terminus of β2, and SII encompasses L4 and α2. The three loops L1 (P-loop), L3 (InterSwitch loop IS), and L7 are colored in blue. GTP is shown in gray. (B) Structural sequence similarity. Plot of the structural sequence similarity SH against the Ras fragment sequence (= $N-3$ residues) for the systems Ras^{U}, $Ras^{PI3K\gamma}$, Ras^{Byr2}, $Ras^{PLC\varepsilon}$, and Ras^{RalGDS}. SH values close to 1 indicate similar local conformations and values close to 0, dissimilar local conformations. SH values were computed for pairs of simulation replicates as indicated by the color scheme in the legend. Dotted gray lines represent a heuristic 0.8 threshold below which fragments are considered to sample significantly different local conformations in the two compared trajectories.

corresponding subtrees, $CD = |h(A) - h(C)| + |h(B) - h(C)|$, where C is the smallest subtree that includes both A and B (Figure S1A,B,C). Whereas ΔCS captures the difference between the widths of two sampled conformational spaces, CD reflects differences between sampled ensembles of the two compared systems. Because CD is computed relatively to the height of the subtrees, it is sensitive to the convergence of the systems. CD values range from 0 to 2.

The two parameters ΔCS and CD are correlated. If the two subtrees do not overlap as in Figure S1A,B, then $CD > \Delta CS$. In the case of low A- and B-subtrees (convergence in both systems), the CD value is large, dominated by the ensemble differences between A and B; this indicates a true conformational change as shown in Figure S1A. However, if A- and B-subtrees are high (both systems unconverged), CD is bound to a small value, and conformational change cannot be reliably inferred, as shown in Figure S1B. If the subtrees of A and B overlap (one system unconverged) as shown in Figure S1C, then $CD = \Delta CS$. In this case, CD is dominated by the sampling width of one system and cannot be reliably attributed to a conformational change.

The interdependence of ΔCS and CD is summarized in Figure S1D. All fragments satisfying the condition $CD = \Delta CS$ (c) are located on the diagonal (dashed gray line), while the fragments satisfying the condition $CD > \Delta CS$ are located above the diagonal (a,b). Therefore, residues undergoing conformational change can be readily identified as off-diagonal points with large CD (a). A heuristic threshold of 0.2 for the selection of data was applied to ΔCS and CD and to the condition $CD > \Delta CS$.

In order to perform a comprehensive comparison of the conformational variation at each position across all systems, a hierarchical clustering approach was used. For each of the 163 fragments of Ras, distances between all pairs of trajectories were computed on the basis of the SH values, and 163 UPGMA trees were built.

Software. Analysis programs were written in Python. Statistical analyses and plots were performed using the R

dx.doi.org/10.1021/ct3007265 | J. Chem. Theory Comput. 2013, 9, 738−749

environment.[41] VMD 1.8.6[42] was used to create structure images.

RESULTS

Overview of Ras Structure and Simulations. The structure of Ras is divided into two parts, the catalytic domain (residues 1−166) and the membrane targeting Hyper Variable Region (HVR; variable length) that anchors the catalytic domain in the membrane. This paper is only concerned with the catalytic domain and its effector complexes, and the term "Ras" will be used synonymously with the catalytic domain. The catalytic domain consists of a central six stranded β-sheet (β1−β6), five α-helices (α1−α5), and 10 loops (L1−L10; Figure 1A). It is dissected into two lobes based on sequence variation between the Ras-isoforms (H-, N-, and K-Ras being the most studied). Lobe 1 (residues 1−86), the effector interaction lobe, is strictly conserved among the isoforms and comprises the P-loop (L1, residues 10−17), switch I (SI, residues 25−40), switch II (SII, residues 57−75), and InterSwitch β2/β3 hairpin (IS, residues 46−49), which connects SI and SII. Lobe 2 (residues 87−166), the membrane linkage lobe, shows sequence variability between the functionally distinct Ras isoforms. Ras GTPases are constitutively bound to a GTP or GDP nucleotide, which is embedded between the P-loop, SI, and SII. The functional loops SI, SII, and L1 show slow interconversions among multiple conformations in the GTP-bound state (millisecond time-scale).[43] Five different Ras systems were analyzed: Ras free, Ras:PI3Kγ, Ras:Byr2, Ras:PLCε, and Ras:RalGDS (":" denotes a complex). Backbone RMSDs between the starting conformations of the Ras domain in the free form and in the different bound forms vary between 0.51 and 0.58 Å. The highly dynamic nature of these systems requires extensive sampling of their accessible conformational space. Three 100 ns MD simulation replicates of five different systems were performed. The conformations of the Ras domain in the trajectories of the free and complexed states were compared to determine how effector interactions modulate the conformation of Ras. We distinguish two levels of structure comparison, global and local. Global analysis comprises the entire structure, while local analysis focuses on the conformation of one to several residues. The global comparison methods, RMSD analysis (Table S1), conformational clustering, and contact maps (data not shown), revealed that the Ras structure is relatively stable with average backbone RMSDs of 0.8−1.3 Å between simulation replicates of the same system. Additionally, the average RMSD of 1.3 Å computed on the combined 15 trajectories illustrates low structural variation between the different systems.

Given the relatively small global structural variation of Ras, effector-induced conformational changes within the simulation time scale of 100 ns are rather to be found at the local level. However, detection of local conformational differences between two distinct systems requires a careful evaluation of sampling variation between the replica simulations of each system; otherwise differences in sampling width might be interpreted as conformational differences. In this study, we propose a procedure to compare MD trajectories of the Ras systems in terms of local conformational differences that takes into account variation of the sampling width within the replicates of each system. The approach is outlined in the following section and explained in technical detail in the Methods.

Local Structure Comparison. Local structures of Ras were compared by translating each structure into a string of letters via a structural alphabet, where each letter represents the backbone conformation of fragments composed of four consecutive residues.[38] This translation has two effects: first, trivial roto-translations are removed and, second, the backbone conformations are coarse-grained into a set of 25 canonical states, which allows for a rapid conformational comparison by string matching. Structural sequence variation, synonymous with local conformational variation, was quantified by position-specific pairwise comparison of the letter composition of the structural sequence sets using an information-theoretic similarity measure, the sequence harmony (SH) value (see Methods). The SH profiles comparing the three simulation replicates of the individual systems (Figure 1B) show that replicates of $Ras^{PLC\varepsilon}$ were very similar to each other with only a few fragments displaying an SH value <0.8. The other SH profiles show that most of the fragments sample similar conformations in the different replicates except for fragments in the P-loop, SI, SII, α3/L7, and C-terminus. Sampling differences of local conformations between the three simulation replicates is indicative of flexible fragments for which the conformational space is not completely covered by the 100 ns simulated time (unconverged trajectories); uniform sampling in the replicates would yield nearly identical letter compositions (converged trajectories). The flexibility of Ras^{U} is shown in Figure 2 in terms of conformational difference between simulation replicates (Top, SH value; Middle, RMSF) and as B-factor of the reference crystal structure. Differences between trajectories may be the result of incomplete sampling; therefore interpretation of protein dynamics requires a careful distinction between effects caused by true differences and those arising from sampling limitations. We propose here a procedure in which two correlated parameters are used to evaluate dynamical and conformational changes against each other.

Conformational differences between two Ras systems may occur for two reasons: first because of differences in the width of the sampled conformational space, which we denote in the following as ΔCS, and second because of (effector-induced) conformational differences, denoted here as CD. It is nontrivial to discern between these two effects, but using the simulation replicates, one can obtain estimates of their relative magnitude. Using the structural strings of the trajectories, distance trees of the 10 pairs of Ras simulations (three replicates each) were computed, yielding 163 trees (one for each Ras residue). In these trees we define as a signal the conformational distance CD, given by the distance between the root nodes of the replicates of the two systems (see Methods), but CD needs to be evaluated against differences in the sampled space. ΔCS is defined by the relative height difference of the two root nodes, indicating a difference in the sampled conformational space. A plot of CD versus ΔCS provides an intuitive illustration of the use of CD and ΔCS for the comparison of pairs of sampled ensembles (Figure 3). Most fragments (>75%) showed low values in both parameters (ΔCS < = 0.2 and CD < = 0.2) and were deemed insignificant in terms of conformational change. Fragments at ΔCS > 0.2 indicate a significant sampling difference between the two compared systems, which could indicate a change in sampling width induced by effector binding. The most informative data points are the off-diagonal fragments (CD > 0.2 and CD > ΔCS), which represent conformational changes at the given Ras position.

Fragments showing divergent sampled space ΔCS occurred most frequently between the Ras^{B} and Ras^{U} systems. The number of these fragments varied between 31 and 40 (35.5 ±

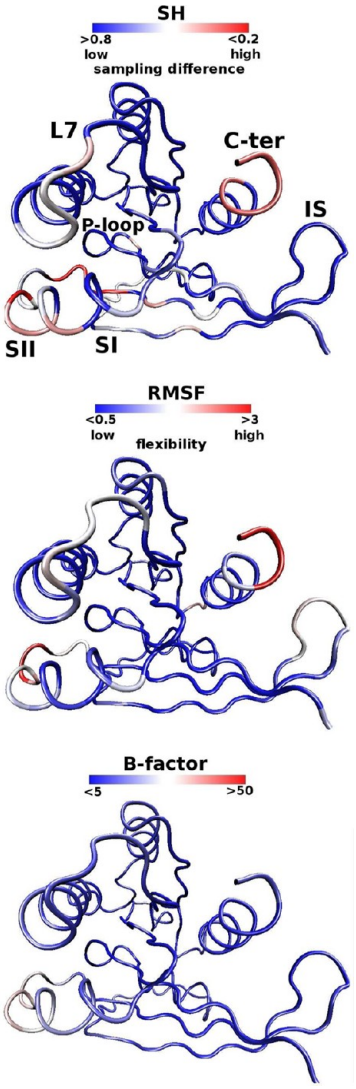

Figure 2. Comparison of SH and RMSF values on Ras structure. Top: SH values were computed between the simulation replicates of Ras^U. For each fragment i (residues i through $i + 3$), the lowest SH value computed between the three pairwise comparisons of the replicates is mapped on the structure at residue $i + 1$. High SH values (blue) indicate low sampling difference; low SH values (red) indicate high sampling difference. Middle: RMSF values on the concatenated three replicates of Ras^U were computed for each residue. High RMSF values (red) indicate high flexibility; low RMSF values (blue) indicate low flexibility. Bottom: B-factors of the X-ray structure of Ras (PDB 1qra) are indicated by the given color range from low (blue) to high (red) values.

3.9) for Ras^U versus Ras^B pairs (Figure 3, bottom row) and between 19 and 33 (27.5 ± 5.6) for Ras^B versus Ras^B pairs (Figure 3, rows 1 to 3). Conversely, conformational changes CD preferentially occurred between the bound systems, involving between 1 and 11 fragments (7.2 ± 3.8). In the following, we first focus on the analysis of fragments with ΔCS > 0.2 to identify regions where the conformational sampling is affected by effector binding. Second, we analyze fragments with conformational changes to identify positions involved in Ras functionality and effector specificity.

Ras Complexation Creates a Rigidified Path from SI to the C-Terminus. Sampling changes upon complexation were analyzed by comparing the four Ras^B systems to the Ras^U reference system. Increased sampling in a Ras^B system compared to Ras^U is denoted as ΔCS^+ and decreased sampling as ΔCS^- .

Complex formation in proteins is often associated with an entropy loss at the binding site due to a loss of degrees of freedom of interacting residues. We detected nine fragments with reduced conformational sampling ΔCS^- in all four effector complexes studied here. These fragments (in parentheses) are located at β1 (f5), SI/β2 (f32, f39), β3/N-terminus of SII (f55, f56), the C-terminus of SII/β4 (f73, f75), and the C-terminus (f161, f162) (Figure 4A). These fragments correspond to residues 5−8 (f5), 32−35 (f32), 39−42 (f39), 55−59 (f55,f56), 73−78 (f73,f75), and 161−165 (f161−f162). Their spatial arrangement forms a path from SI at the binding site to the C-terminus of Ras. This long-range rigidification reaches far beyond the binding site into the structure. Most of this ΔCS^- signal originates from the difference of Ras^B from a single simulation replicate of Ras^U in which SI−Thr35 detached slightly from the γ-P of the nucleotide, increasing the distance from about 4.7 ± 0.3 to 5.5 ± 1.3 Å. Detachment of Ras−Thr35 in SI from the γ-P of the nucleotide is characteristic of Ras state1, which exhibits low effector affinity.[4] The Ras^U conformation clearly features characteristics of state1. The impact of the increased distance between SI-T35 and the γ-P on the rest of the protein structure as observed in the simulation is likely to mimic changes occurring in the state1/state2 transition. Therefore, the differences observed between Ras^U (exploring state1-like conformations) and Ras^B (locking Ras in state2 conformations in all 12 Ras^B simulations) suggests that the observed transmission path overlaps with the conformational changes of Ras associated with the state1/state2 transition.

To support the hypothesis of the transmission path, we analyzed additionally the residue interaction patterns, in particular the contacts that are found in Ras^B but not in Ras^U. The intramolecular contact maps of all five Ras systems are overall very similar, demonstrating a globally stable interaction network largely independent of the complexation state (Figure S2A). However, 12 persistent inter-residue contacts (□ symbols) were found only in the four Ras^B systems (Table S2). These contacts involve residues in β1 (5,7,8), P-loop (17), SI/β2 (34−36,38,40), β3 (55−57), L5/β4 (71,75−77,79), β5 (110), and the C-terminus (162). An almost complete overlap exists between the nine ΔCS^- fragments and the 12 bound-specific contact pairs (Figure 4B): eight ΔCS^- fragments comprise at least one residue involved in a bound-specific contact pair, and 11 contact pairs are part of a ΔCS^- fragment. The implied long-range connection from the binding site to the C-terminus of the catalytic domain is also in agreement with the energetic contribution of C-terminal residues detected in both Ras:RalGDS and Ras:Raf complexes.[16] We deduce that this path might be an intramolecular transmission path of the binding signal.

Possible Functional Role of Ras-SII in Effector Binding. Despite the high flexibility of SII in all simulated Ras systems, differences were detected in this region between Ras^U and Ras^B. While no position showed ΔCS^+ upon interaction with all four effectors, residues around position 66 indicate increased sampling in $Ras^{PI3K\gamma}$, Ras^{Byr2}, and Ras^{RalGDS}. Residues 66−69 form a helical turn of α2, whose unwinding is responsible for the large scale motion of the SII region upon GDP/GTP exchange.[44] Interactions between Ras−SII and regions outside the Ras binding domain of the effectors (only

dx.doi.org/10.1021/ct3007265 | J. Chem. Theory Comput. 2013, 9, 738−749

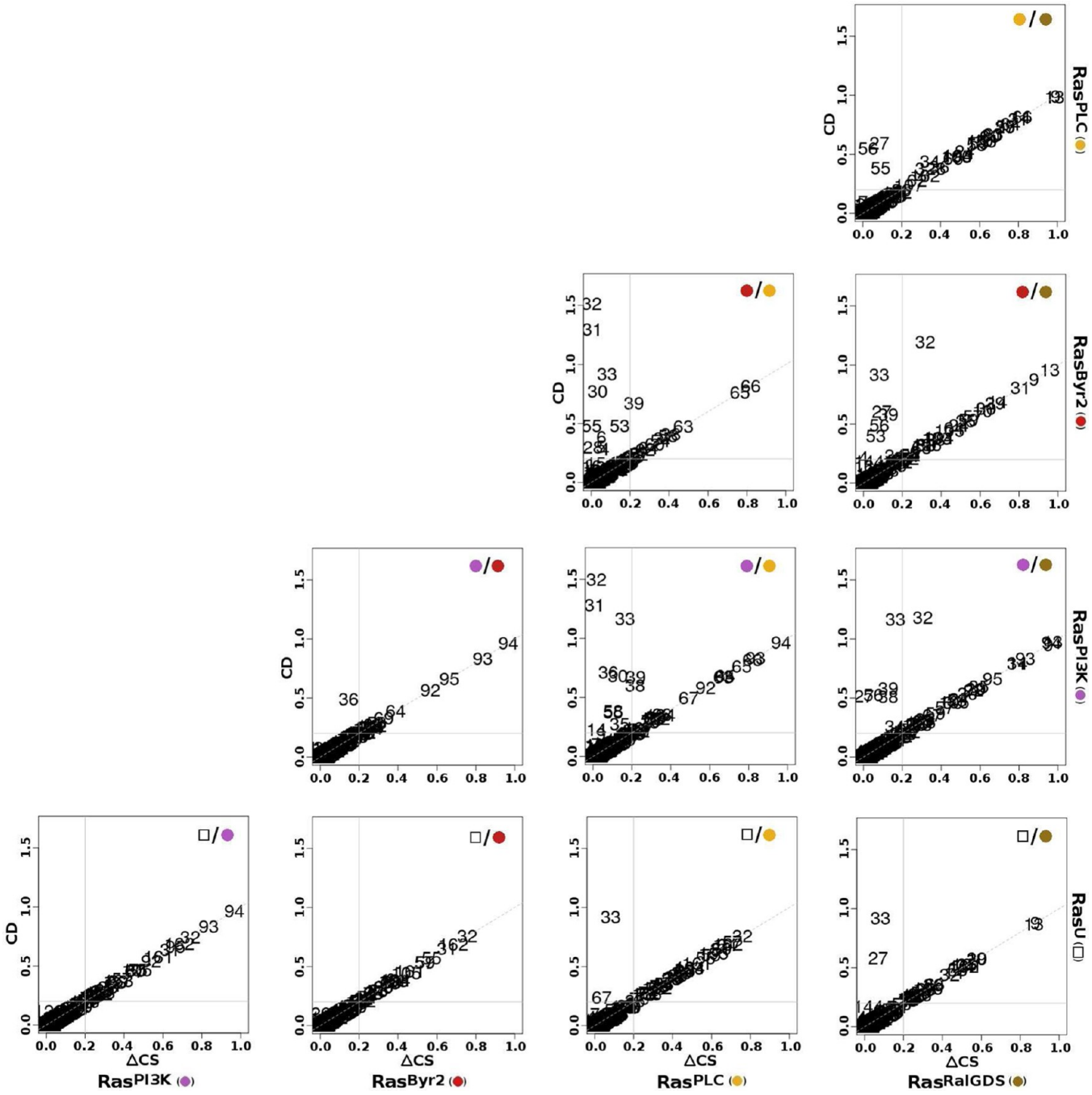

Figure 3. Conformational comparison of Ras systems. CD versus ΔCS plots for all of the Ras fragments of the 10 pairwise comparisons between Ras systems. Each Ras fragment *fi* (residues *i* to *i* + 3) is identified in the plots by its corresponding number *i*. The dotted gray line shows the diagonal CD = ΔCS; a solid gray lines shows the 0.2 thresholds for ΔCS (vertical) and CD (horizontal).

the Ras binding domain of effectors was simulated here) have been previously reported for Ras:PI3Kγ[22] and Ras:RalGDS[45] complexes and have been shown to be critical for RalGDS activation.[45] Whether the increased sampling around position 66 is a compensatory entropic effect to the effector binding or related to putative interactions outside the effector binding site remains yet unresolved.

Specific Conformational Responses of Ras to Effector Binding. To locate specific conformational responses of Ras to effector binding, differences in local conformations between the four Ras^B systems were analyzed. Although the identity of Ras interacting residues is very similar in all bound systems (Figure S2B), we identified 19 fragments with conformational differences between at least two Ras^B systems. They are located in SI/β2 (11 fragments), β1 (4), β3 (3), and P-loop(1) (Figure 5A). Among these fragments, 17 also showed ΔCS$^-$ upon complexation with at least one effector, five (f5, f32, f39, f55, and f56) are part of the transmission path described above, and nine (f34−f36, f38, f39, f55, f56, f4, and f5) contain hot-spot residues for the interaction of Ras with RalGDS and/or Raf (namely, SI/β2 37, 38, 39, and 40; β3 57; and β1 5) in two studies.[16,17] This means that the rigidification of the transmission path upon complexation is combined with changes in the Ras structure toward a narrower effector-specific conforma-

dx.doi.org/10.1021/ct3007265 | J. Chem. Theory Comput. 2013, 9, 738−749

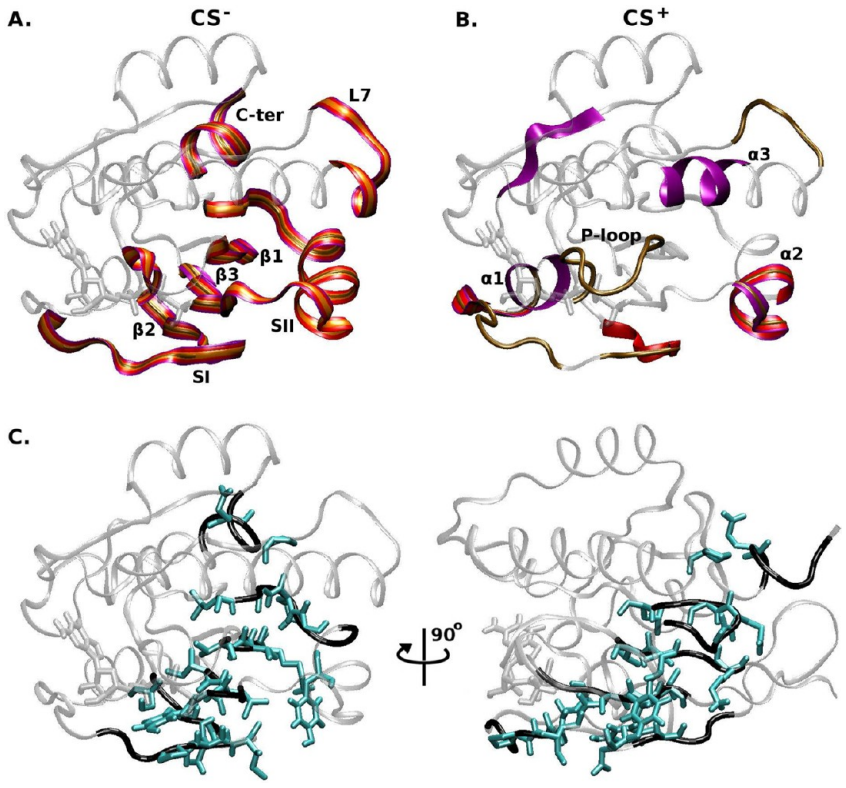

Figure 4. Plot of differences in Ras dynamics. (A) Structure mapping of Ras residues in fragments with reduced (ΔCS^-, left) and increased (ΔCS^+, right) conformational sampling upon complexation with PI3Kγ (purple wide ribbon), Byr2 (red medium size ribbon), PLCε (orange narrow ribbon), and RalGDS (brown line). The rest of the protein as well as GTP are transparent. The ribbon width varies to show the contributing systems, not to reflect parameter scales. Note that a fragment at position i comprises four residues from i to $i + 3$. Therefore, although some residues are highlighted in both structures, they may be part of different fragments. (B) Fragments with ΔCS^- in all bound systems are shown as black tubes on the Ras structure; side chains involved in bound-specific inter-residue contacts are shown as cyan stick models.

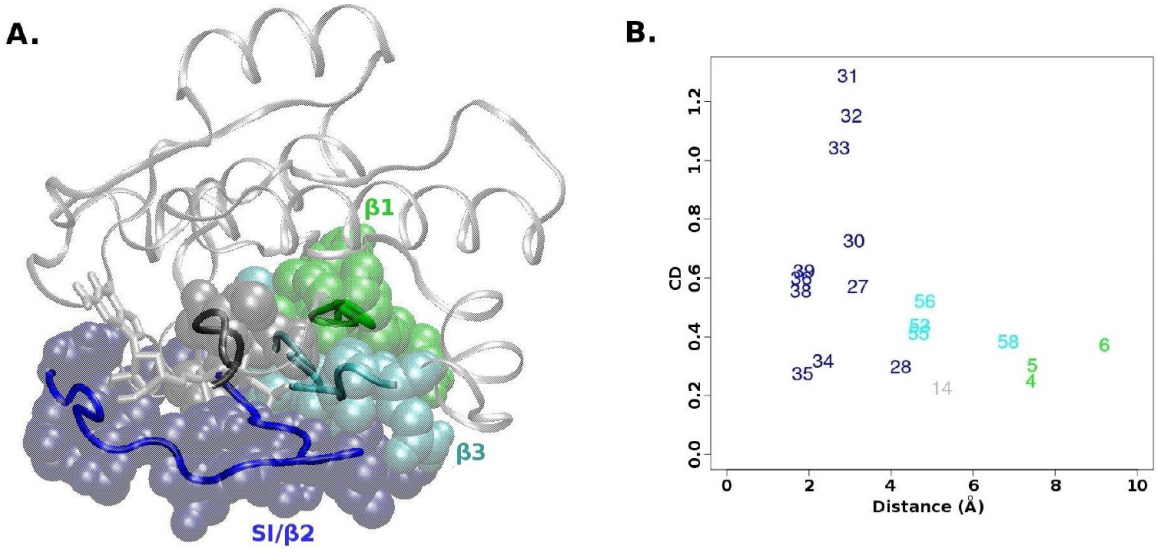

Figure 5. Conformational changes and effector distance. (A) Fragments with conformational changes are colored according to their location in the structure: SI/β2, blue; β3, cyan; β1, green; P-loop, gray. (B) Correlation between the average conformational distance (CD) of systems showing conformational difference and the average distance between the residues of the fragment and the effectors.

tional space. The binding signal propagates from SI/β2 to β3 and β1, where hot-spot residues for the interface have been previously predicted,[16,17] namely Ras residues Y5 and D57.

These findings point toward an activation mechanism including equilibrium dynamics between various conformers of Ras^U and conformational selection upon effector binding, as proposed in ref 25 and supported by our simulations. The SI/β2 region, which forms the strongest and direct contacts with the effectors, displays the largest conformational differences. The conformational effect of the effectors on the Ras structure tends to decrease with increasing distance from the interface (Figure 5B). Although SII forms contacts with the effectors, no

dx.doi.org/10.1021/ct3007265 | J. Chem. Theory Comput. 2013, 9, 738−749

effector specific conformational differences were detected in this region.

According to the SMART database,[46,47] effectors RalGDS and PLCε belong to the RA domain family,[9] whereas PI3Kγ and Byr2 are associated with other types of domains: PI3Kγ is classified as PI3K-RBD in the SMART database; Byr2 is a functional homologue of the RB domain Raf. We compared the conformational changes induced by the RA domain effectors Ras^{RalGDS} and $Ras^{PLC\varepsilon}$ with those induced by the non-RA domain effectors $Ras^{PI3K\gamma}$ and Ras^{Byr2}. We identified three fragments f32, f33, and f39 on SI/β2 (Figure 6), which show among the largest conformational differences.

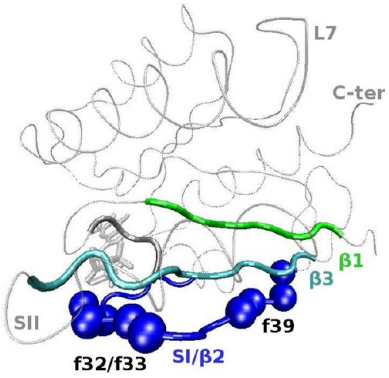

Figure 6. Location of f32, f33, and f39 on the Ras structure. The three fragments f32, f33, and f39 (C^{α} atoms in VdW representation), which adopt distinct conformations upon RA and non-RA domain binding, are located on SI/β2 (blue). Other fragments detected with conformational changes are represented as in Figure 4A.

The backbone conformations of f39 are illustrated in Figure 7A. In the effector complex, the Ras backbone at S39 forms hydrogen bonds with the backbone of the equivalent β2 residues of the different effectors (namely, RalGDS−R20, PLCε−Y31, PI3Kγ−S230, and Byr2−T82). The different side chain length in the domain types (R,Y versus S,T) induces distinct steric constraints on Ras. The interaction pattern of Ras−Y40 depends on the effector domain type (Figure 7B). The Y40 interacting effector residues of the RA domains (PLCε−Q18 and RalGDS−N29) are located two residues after those of the equivalent residues of the non-RA domains (PI3Kγ−Q231 and Byr2−R83). The two interaction patterns invoke different structural restraints: RA domains induce a bending of the backbone of the effector's β2 strand; non-RA domains induce a torsion of the Ras backbone (Figure S3). The importance of f39 for effector binding and specificity is supported by mutational analysis. Ras mutations S39P and Y40K abrogate the interaction between Ras and Byr2;[13] Ras mutation Y40C[22] reduces the binding of Ras to effectors containing Glu as an interacting residue (PI3Kγ and isoform PI3Kδ). Byr2−R83 is required for the binding of Byr2 to Ras, but mutation of the equivalent residue RalGDS−K32 to Ala only reduces the binding affinity.[11]

The other two fragments that appear to convey effector domain specificity are f32 and f33 (Figure 8A). T35 is oriented toward the GTP and coordinates the Mg^{2+} ion; D33 forms a negatively charged groove with D38 that accommodates an α1−Lys of the effector (Figure 8B). Although Ras−T35 is located at the same position in all complexes, Ras−D33 adopts a position depending on the effector domain type. There is no

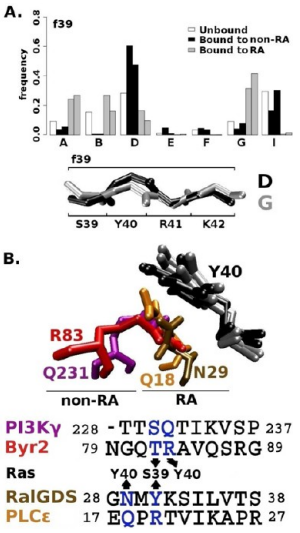

Figure 7. Conformations and interactions at the segment S39−K42. (A) Relative frequencies of local conformations of f39 along the three simulation replicates of Ras^{U} (white), $Ras^{PI3K\gamma}$, and Ras^{Byr2} (non-RA domains, black) and $Ras^{PLC\varepsilon}$ and Ras^{RalGDS} (RA domains, gray). The backbone of Ras−39-to-42 is shown in the preferred conformation: G conformation when bound to a RA domain and D conformation when bound to a non-RA domain. (B) non-RA domain residues PI3Kγ−S230 and Byr2−T82 and RA domain residues RalGDS−R20 and PLCε−Y31 occupy the space around Ras−Y40, but the side chain has a different orientation. Alignment of the β2 sequence of all effectors is given with interacting residues in blue. The conformations of f39 in the starting structures were □ A, ■ A/B, and gray-filled □ B.

apparent reason why the direct interaction of the Lys residues with Ras−D33 should differ, but the flanking Lys residues in non-RA domains (PI3Kγ−K254 and Byr2−K100; bottom sequences in Figure 8B) could be the cause. Removing or adding Lys at the flanking position affects effector binding: mutation PI3Kγ−K254A lowers the affinity of PI3Kγ to Ras, although it does not interact directly with Ras,[22] and mutation RalGDS−D51K increases the affinity of RalGDS to Ras.[11] It has been suggested that the additional Lys in PI3Kγ restrains the flexibility in the turn containing PI3Kγ−K255, thereby favoring the interaction between the effector and Ras.[22] In agreement with these results, we found that the average distance between the effector's NZ atom of α1-Lys and the CG atom of Ras−D33 was about 1−2 Å longer in RA domains (6.5 ± 1.8 Å in Ras:PLCε, 5.4 ± 1.4 Å in Ras:RalGDS) compared to non-RA domains (4.6 ± 1.1 Å in Ras:PI3Kγ, 4.1 ± 0.9 Å in Ras:Byr2).

A truly effector specific behavior was exhibited by fragment f36. In the unbound form or complexed with RalGDS, a wide range of states was sampled (mainly E/C/B/Q), fewer states when complexed to Byr2 (mainly M/C/E) and PLCε (mainly E/B), and even fewer with PI3Kγ (mainly Q). Mutation of Ras residues E37 and D38, comprised in f36, have been reported to affect the binding of Ras in an effector specific manner.[10,13,22,48,49] Pacold et al.[22] determined the reason for the differential effects of the Ras−D38E mutation on the binding to Raf, PI3Kγ, and RalGDS: the space filled by the larger mutant side chain E38 is occupied in the native structure by effector residues with different properties in terms of size/polarity. The individual specificities of the effectors induce specific local adaption of the Ras backbone, resulting in conformational differences at f36 that were also detected here.

dx.doi.org/10.1021/ct3007265 | J. Chem. Theory Comput. 2013, 9, 738−749

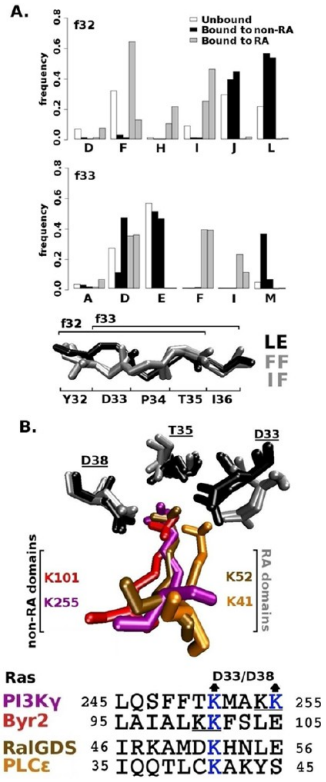

Figure 8. Conformations and interactions at the segment Y32−I36. (A) Relative frequencies of local conformations of f32 and f33 along the three simulation replicates of Ras^{U} (white), $Ras^{PI3K\gamma}$, and Ras^{Byr2} (non-RA domains, black) and $Ras^{PLC\varepsilon}$ and Ras^{RalGDS} (RA domains, gray). The backbone of Ras−32-to-36 is shown in the preferred conformation when bound to RA/non-RA domains. (B) Structural comparison of the α1-Lys of the effectors that binds to the negatively charged groove formed by Ras−D33 and D38. Ras−T35 is also shown. Bottom: Alignment of the C-terminal sequence of the effectors. Interacting residues of α1 are colored blue. The double Lys motif of the non-RA domains is underlined. The conformations of f32 in the starting structures were □ D, ■ F, and gray-filled □ F/D; those of f39 were □ D, ■ D/F, and gray-filled □ D.

■ DISCUSSION

In this study, we presented a comparison of the dynamics of Ras-GTPase loaded with GTP in five different states, unbound and bound to the effectors PI3Kγ, RalGDS, PLCε, and Byr2. The data provided a wealth of information regarding the associated conformational ensembles. By introducing a procedure to quantify local conformational changes, conformational differences were detected between the bound and unbound states as well as between the bound states. These conformational analyses provided clues about some mechanistic aspects of the function of Ras, based on several residues showing either modified sampling width or conformational changes upon binding. These results suggest a nucleotide independent mechanism that is probably related to the state1/state2 transition of Ras (discussed below). Effector binding not only locks Ras in state2 by rigidifying SI, it also propagates conformational changes along a path from SI to the C-terminus (residues 5−8, 32−35, 39−42, 55−59, 73−78, and 161−165), which embeds 12 bound-specific contact pairs (residues 5, 7, 8, 17, 34−36, 38, 40, 55−57, 71, 75−77, 79, 110, and 162). The rigidification of this path is associated with conformational changes that are specifically influenced by the bound effector. These findings suggest a conformational selection mechanism in which the complex conformation modulates the functional response of Ras to the binding event. Among the 19 fragments showing conformational differences between the bound forms of Ras at the N-terminus of the central β-sheet were some residues that were noticed in previous mutation experiments and *in silico* studies: fragments 4 and 56 encompass noninterface residues Y5 and D57 that were predicted as hot-spot residues in Ras:Raf and Ras:RalGDS;[16,17] f36 encompasses residues E37 and D38 that affect Ras binding depending on the effector bound.[10,13,22,48,49] However, several positions have not been detected before, for example Ras residues involved in the propagation of the binding signal along the central β-sheet from interacting residues to hot-spot residues (residues in f53/f4 and f34/f56) and residues in f32, f33, and f39 involved in the distinction between RA-domain and non-RA domain effectors.

Effector complexation of Ras-GTP leads to a reduced flexibility of a series of proximal residues, forming a structural path from the SI region to the α5 helix at the C-terminus through the central β-sheet. This dynamical change appears to prevent the detachment of SI from the guanosine nucleotide upon binding. Such a detachment observed in Ras-GTP state1[4] is associated with low effector binding affinity.[3] While the unbound form of Ras-GTP is able to explore both state1 and state2, the closed conformation of active Ras-GTP state2 was previously shown to be stabilized upon complexation.[50,51] Our results show how effector binding locks Ras-GTP in its active state2 conformation by rigidifying not only SI but several interacting parts of the Ras structure linking SI to the α5 helix, where residues have been shown to contribute to the binding energy of the complexes.[16] This clearly suggests a functional role for this path in the state1/state2 transition. A dynamical linkage between the nucleotide-binding site formed by the switch regions and the membrane interacting C-terminus have been previously reported to be critical for the GDP/GTP conformational state transition of Ras superfamily members[5,52] and for effector binding.[6,7] The C-terminal helix α5 is involved in a nucleotide-dependent conformational switch that permits the GTP-loaded catalytic domain of Ras to adopt a specific orientation with respect to the membrane that is sterically more favorable for effectors to bind. Nucleotide-dependent changes of Ras were excluded here, because all simulations presented in this study were performed on Ras GTP-loaded systems. Despite that, a path similar to the nucleotide-induced one was detected by comparing the bound (locked in state2) and unbound (exploring state1-like and state2 conformations) Ras GTP-loaded systems. This suggests an overlap between the mechanisms governing the transition upon GTP binding and the state1/state2 transition. Our results and previous studies support this hypothesis. For instance, the conformational changes of the nucleotide binding site accompanying state1/state2 transition have been shown to mimic those occurring upon GDP/GTP exchange,[4] and Ras state1 was suggested to be an intermediate state of the nucleotide exchange process.[53] Therefore, the conformational changes at the binding sites during the state1/state2 transition are likely to affect the rest of the protein in a similar manner as during the GDP/GTP exchange. Furthermore, the C-terminus of Ras has been suggested to have a regulatory effect on the state1/state2 conformational equilibrium.[54] As further evidence for the role of the C-terminus of Ras in the state1/state2 transition, here we identified a path between SI and α5 whose dynamics are altered when Ras is locked in state2 upon effector binding.

dx.doi.org/10.1021/ct3007265 | J. Chem. Theory Comput. 2013, 9, 738−749

The SII region displays a complicated dynamic picture with various effector-specific effects upon complexation. The increased local flexibility observed in the SII region of $Ras^{PI3K\gamma}$, Ras^{Byr2}, and Ras^{RalGDS} could reflect an important role of SII in the binding and activation of these effectors by forming contacts with the effectors in regions outside the canonical Ras binding domain.[22,45] Contrastingly, the $Ras^{PLC\varepsilon}$ complex is locally and globally more rigid than Ras alone. Changes of flexibility in complexes have been shown to be associated with the activation of downstream effectors in other proteins of the Ras superfamily.[26] Hota et al.[26] underline that changes in flexibility could be responsible for different functional behavior, preventing or favoring the small GTPases to form additional interactions with other regions than the canonical binding domain of the effectors or with other proteins. We assume that the differences in local and global flexibility observed here between the four Ras:effector complexes reflect differences in these noncanonical binding regions.

Besides the changes in flexibility, conformational adaptations of Ras to the specific structural constraints of the effectors were observed. In particular, regions of SI/β2 (residues 32−36 and 39−41) adopted different states when bound to RA or non-RA type effector domains. These differences were shown to be due to domain-specific interactions between the effectors and Ras−Y40/D33. RA/RB domain-specific modes of binding have been suggested by Kiel et al.,[19] who report different energy landscapes at the interface of Ras:RalGDS (RA domain) and Ras:Raf (RB domain) complexes. Domain types are shown here to be associated with specific local conformations. True Ras binding domains (i.e., those known to interact with active Ras as opposed to putative Ras binding domains that contain the RA or RB sequence motif) of different types have been defined.[11,12] A comprehensive analysis of Ras conformations in complexes with these "true" domains would be of great interest for the classification of effectors. The low sequence similarity between Ras binding domain families render their classification difficult; analyses on structure/function relationships could provide characteristic features.

■ ASSOCIATED CONTENT

Supporting Information

Sampling width and conformational change (Figure S1). Contact maps (Figure S2). Conformations and interactions at Y40 (Figure S3). Average and maximum RMSD values (in Å) of the Ras backbone in Ras^{U}, $Ras^{PI3K\gamma}$, Ras^{Byr2}, $Ras^{PLC\varepsilon}$, and Ras^{RalGDS} (Table S1). Average distance and standard deviation (in Å) between pairs of residues in Ras^{U}, $Ras^{PI3K\gamma}$, Ras^{Byr2}, $Ras^{PLC\varepsilon}$, and Ras^{RalGDS} (Table S2). This information is available free of charge via the Internet at http://pubs.acs.org/.

■ AUTHOR INFORMATION

Corresponding Author

*E-mail: jbaussa@nimr.mrc.ac.uk.

Notes

The authors declare no competing financial interest.

■ ACKNOWLEDGMENTS

We thank A. Ridley, F. Fraternali, and M. Sadowski for helpful suggestions. J.B. acknowledges support by ESF (Exchange grant 2192) in collaboration with A.C. Camproux, by EMBO (ALTF651-2009), and by the MRC. J.K. acknowledges support by the MRC National Institute for Medical Research (U117581331).

■ ABBREVIATIONS

PI3Kγ, phosphoinositide 3-kinase γ; RalGDS, Ral guanine nucleotide dissociation stimulator; PLCε, phospholipase Cε; GDP, guanosine diphosphate; GTP, guanosine triphosphate; SI, switch I region; SII, switch II region; IS, interswitch region; RA, Ras association domain; RB, Ras binding domain; Ras^{U}, Ras unbound; Ras^{B}, Ras bound to unspecified effector; Ras^{X}, Ras bound to effector *X*

■ REFERENCES

(1) Schubbert, S.; Shannon, K.; Bollag, G. *Nat. Rev. Cancer* **2007**, *7*, 295−308.
(2) Corbett, K.; Alber, T. *Trends Biochem. Sci.* **2001**, *26*, 710−716.
(3) Spoerner, M.; Herrmann, C.; Vetter, I. R.; Kalbitzer, H. R.; Wittinghofer, A. *Proc. Natl. Acad. Sci. U. S. A.* **2001**, *98*, 4944−4949.
(4) Shima, F.; Ijiri, Y.; Muraoka, S.; Liao, J.; Ye, M.; Araki, M.; Matsumoto, K.; Yamamoto, N.; Sugimoto, T.; Yoshikawa, Y.; Kumasaka, T.; Yamamoto, M.; Tamura, A.; Kataoka, T. *J. Biol. Chem.* **2010**, *285*, 22696−22705.
(5) Grant, B. J.; Gorfe, A. A.; McCammon, J. A. *PLoS Comput. Biol.* **2009**, *5*, e1000325.
(6) Abankwa, D.; Hanzal-Bayer, M.; Ariotti, N.; Plowmanmpm, S. J.; Gorfe, A. A.; Parton, R. G.; McCammon, J. A. *EMBO J.* **2008**, *27*, 727−735.
(7) Abankwa, D.; Gorfe, A. A.; Hancock, J. F. *Cell Cycle* **2008**, *7*, 2667−2673.
(8) Abankwa, D.; Gorfe, A. A.; Inder, K.; Hancock, J. F. *Proc. Natl. Acad. Sci. U. S. A.* **2010**, *107*, 1130−1135.
(9) Ponting, C. P.; Benjamin, D. R. *Trends Biochem. Sci.* **1996**, *21*, 422−425.
(10) Rodriguez-Viciana, P.; Sabatier, C.; McCormick, F. *Mol. Cell. Biol.* **2004**, *24*, 4943−4954.
(11) Wohlgemuth, S.; Kiel, C.; Krämer, A.; Serrano, L.; Wittinghofer, F.; Herrmann, C. *J. Mol. Biol.* **2005**, *348*, 741−758.
(12) Kiel, C.; Wohlgemuth, S.; Rousseau, F.; Schymkowitz, J.; Ferkinghoff-Borg, J.; Wittinghofer, F.; Serrano, L. *J. Mol. Biol.* **2005**, *348*, 759−775.
(13) Akasaka, K.; Tamada, M.; Wang, F.; Kariya, K.; Shima, F.; Kikuchi, A.; Yamamoto, M.; Shirouzu, M.; Yokoyama, S.; Kataoka, T. *J. Biol. Chem.* **1996**, *271*, 5353−5360.
(14) Heo, W. D.; Meyer, T. *Cell* **2003**, *113*, 315−328.
(15) Gohlke, H.; Kuhn, L. A.; Case, D. A. *Proteins* **2004**, *56*, 322−337.
(16) Gohlke, H.; Kiel, C.; Case, D. A. *J. Mol. Biol.* **2003**, *330*, 891−913.
(17) Tomić, S.; Bertosa, B.; Wang, T.; Wade, R. C. *Proteins* **2007**, *67*, 435−447.
(18) Rudolph, M. G.; Linnemann, T.; Grünewald, P.; Wittinghofer, A.; Vetter, I. R.; Herrmann, C. *J. Biol. Chem.* **2001**, *276*, 23914−23921.
(19) Kiel, C.; Serrano, L.; Herrmann, C. *J. Mol. Biol.* **2004**, *340*, 1039−1058.
(20) Vetter, I. R.; Linnemann, T.; Wohlgemuth, S.; Geyer, M.; Kalbitzer, H. R.; Herrmann, C.; Wittinghofer, A. *FEBS Lett.* **1999**, *451*, 175−180.
(21) Wittinghofer, A.; Waldmann, H. *Angew. Chem., Int. Ed.* **2000**, *39*, 4192−4214.
(22) Pacold, M. E.; Suire, S.; Perisic, O.; Lara-Gonzalez, S.; Davis, C. T.; Walker, E. H.; Hawkins, P. T.; Stephens, L.; Eccleston, J. F.; Williams, R. L. *Cell* **2000**, *103*, 931−943.
(23) Scheffzek, K.; Grünewald, P.; Wohlgemuth, S.; Kabsch, W.; Tu, H.; Wigler, M.; Wittinghofer, A.; Herrmann, C. *Structure* **2001**, *9*, 1043−1050.
(24) Fuentes, G.; Valencia, A. *Trends Biochem. Sci.* **2009**, *34*, 533−539.

(25) Arai, Y.; Iwane, A. H.; Wazawa, T.; Yokota, H.; Ishii, Y.; Kataoka, T.; Yanagida, T. *Biochem. Biophys. Res. Commun.* **2006**, *343*, 809−815.
(26) Hota, P. K.; Buck, M. *Protein Sci.* **2009**, *18*, 1060−1071.
(27) Filchtinski, D.; Sharabi, O.; Rüppel, A.; Vetter, I. R.; Herrmann, C.; Shifman, J. M. *J. Mol. Biol.* **2010**, *399*, 422−435.
(28) Scheidig, A. J.; Burmester, C.; Goody, R. S. *Structure* **1999**, *7*, 1311−1324.
(29) Huang, L.; Hofer, F.; Martin, G. S.; Kim, S. H. *Nat. Struct. Biol.* **1998**, *5*, 422−426.
(30) Bunney, T. D.; Harris, R.; Gandarillas, N. L.; Josephs, M. B.; Roe, S. M.; Sorli, S. C.; Paterson, H. F.; Rodrigues-Lima, F.; Esposito, D.; Ponting, C. P.; Gierschik, P.; Pearl, L. H.; Driscoll, P. C.; Katan, M. *Mol. Cell* **2006**, *21*, 495−507.
(31) Sali, A.; Blundell, T. L. *J. Mol. Biol.* **1993**, *234*, 779−815.
(32) Shen, M.-Y.; Sali, A. *Protein Sci.* **2006**, *15*, 2507−2524.
(33) Hess, B.; Kutzner, C.; van der Spoel, D.; Lindahl, E. *J. Chem. Theory Comput.* **2008**, *4*, 435−447.
(34) Berweger, D.; van Gunsteren, W. F.; Müller-Plathe, F. *Chem. Phys. Lett.* **1995**, *232*, 429−436.
(35) Berendsen, H. J. C.; Postma, J. P. M.; van Gunsteren, W. F.; Di Nola, A.; Haak, J. R. *J. Chem. Phys.* **1984**, *81*, 3684−3690.
(36) Ryckaert, J.-P.; Ciccotti, G.; Berendsen, H. J. C. *J. Chem. Phys.* **1977**, *23*, 327−341.
(37) Gorfe, A. A.; Grant, B. J.; McCammon, J. A. *Structure* **2008**, *16*, 885−896.
(38) Pandini, A.; Fornili, A.; Kleinjung, J. *BMC Bioinf.* **2010**, *11*, 97.
(39) Pirovano, W.; Feenstra, K. A.; Heringa, J. *Nucleic Acids Res.* **2006**, *34*, 6540−6548.
(40) Michener, C.; Sokal, R. *Evolution* **1957**, *11*, 490−499.
(41) *R: A Language and Environment for Statistical Computing*; R Foundation for Statistical Computing: Vienna, Austria, 2010.
(42) Humphrey, W.; Dalke, A.; Schulten, K. *J. Mol. Graphics* **1996**, *14*, 33−38.
(43) Ito, Y.; Yamasaki, K.; Iwahara, J.; Terada, T.; Kamiya, A.; Shirouzu, M.; Muto, Y.; Kawai, G.; Yokoyama, S.; Laue, E.; Wülchli, M.; Shibata, T.; Nishimura, S.; Miyazawa, T. *Biochemistry* **1997**, *36*, 9109−9119.
(44) Ma, J.; Karplus, M. *Proc. Natl. Acad. Sci. U. S. A.* **1997**, *94*, 11905−11910.
(45) Linnemann, T.; Kiel, C.; Herter, P.; Herrmann, C. *J. Biol. Chem.* **2002**, *277*, 7831−7837.
(46) Schultz, J.; Milpetz, F.; Bork, P.; Ponting, C. P. *Proc. Natl. Acad. Sci. U. S. A.* **1998**, *95*, 5857−5864.
(47) Letunic, I.; Doerks, T.; Bork, P. *Nucleic Acids Res.* **2009**, *37*, D229−D232.
(48) White, M.; Nicolette, C.; Minden, A.; Polverino, A.; Van Aelst, L.; Karin, M.; Wigler, M. *Cell* **1995**, *80*, 533−541.
(49) Rodriguez-Viciana, P.; Warne, P. H.; Khwaja, A.; Marte, B. M.; Pappin, D.; Das, P.; Waterfield, M. D.; Ridley, A.; Downward, J. *Cell* **1997**, *89*, 457−467.
(50) Geyer, M.; Herrmann, C.; Wohlgemuth, S.; Wittinghofer, A.; Kalbitzer, H. R. *Nat. Struct. Biol.* **1997**, *4*, 694−699.
(51) Huber, F.; Grrünewald, P.; Sprörner, M.; Wohlgemuth, S.; Herrmann, C.; Kalbitzer, H. R. *Structure* **2001**, *9*, 1029−1041.
(52) Grant, B. J.; McCammon, J. A.; Gorfe, A. A. *Biophys. J.* **2010**, *99*, L87−L89.
(53) Kobayashi, C.; Saito, S. *Biophys. J.* **2010**, *99*, 3726−3734.
(54) Spoerner, M.; Hozsa, C.; Poetzl, J. A.; Reiss, K.; Ganser, P.; Geyer, M.; Kalbitzer, H. R. *J. Biol. Chem.* **2010**, *285*, 39768−39778.